M Roldan et al.

Deformation behaviour and microstructural evolution of EUROFER97-2 under Low Cycle Fatigue conditions

Deformation behaviour and microstructural evolution of EUROFER97-2 under Low Cycle Fatigue conditions

M. Roldán [(1)*], *E. Leon-Gutierrez* [(1)], *P. Fernández* [(1)], *A. Gómez-Herrero* [(2)].

[1] *CIEMAT. National Fusion Laboratory. Technology Division. Avda. Complutense, 40. 28040. Madrid. Spain.*

[2] *National Center for Electronic Microscopy. Avda. Complutense s/n. 28040. Madrid. Spain*

Corresponding author: marcelo.roldan@ciemat.es

1. ABSTRACT

Low cycle fatigue (LCF) behavior of version 2, EUROFER97 was studied in normalized plus tempered condition within a wide total strain range from 0.4 to 1.8 % at RT and 550 ºC. At the lowest strain (0.4%) EUROFER97-2 shows very low softening behavior at both temperatures, however, increasing the strain amplitude, the material showed an instant hardening followed by a sharp softening up to rupture, fatigue life being reduced. Deep microstructural characterization by STEM in thin foils and also in carbon extraction replica was performed on selected samples strained at 0.4, 0.8, 1 and 1.8 % at RT and 550 ºC, respectively. The microstructural development is based on dislocations rearrangement and/or annihilation which finally lead to sub-grain formation and growth, specially enhanced at 550ºC. The microstructural modifications, concerning dislocations and sub-grain structures, are more intense as the strain amplitude applied increase. No significant change of composition, size and distribution of $M_{23}C_6$ and MX precipitates was observed. Consequently, the fatigue life of EUROFER97-2 at room temperature and at 550ºC is strongly dependent of dislocation evolution.

2. INTRODUCTION

The structural components of the future fusion reactors will be subjected to thermal stresses as a result of temperature gradients. Therefore LCF assume special relevance in the safe life approach on fusion components.

In the framework of Fusion Power plant design in Europe, the next step is the design of structural components of the European Demonstration Power Plant (EU-DEMO). Nuclear fusion energy production requires design criteria developed specifically for those components and severe conditions of operation. Therefore the verification of a blanket design for demonstration power plant has to be based on a consistent set of rules recorded on a nuclear code. The purpose of the design rules is to ensure that the

required safety margins are maintained relative to the types of mechanical damage which might occur.

The structure and the environment of the structural components of fusion reactors have unique features that require special consideration; plasma disruptions producing transient of dynamical and thermal stresses, mechanical properties degradation due to the irradiation and the use of new materials; Reduced Activation Ferritic/Martensitic steels (RAFM steels). All these factors require the use a multi-code approach based on ASME[1], SDC-IC [2], RCC-MR [3] and RCC-MRx (in development) [4], because the current existing industrial codes are no able to cover all the fusion features by only one. To establish the design rule (criteria to prevent failure), it is necessary to identify the possible failure modes taking into account the operation conditions and the mechanical properties of the selected material. In the context of DEMO in-vessel components, among others, one of the key failure mode identified is fatigue [5].

The European Fusion materials community has been characterizing the reduced activation martensitic steel called EUROFER97 since two decades because it has been selected as reference structural material for fusion applications to build the European TBMs for ITER [6-8], with perspective to be used in DEMO. The selection of this material is due to its reduced activation potential, high temperature of operation, good corrosion resistance and good behavior under neutron and ion [9, 10] irradiation [11, 12]. Its mechanical properties were collected and analyzed to create databases in order to can include the material properties of EUROFER97 in the RCC-MRx code [13]. Low cycle fatigue (LCF) tests were performed on the as received state and after neutron irradiation in the past to address the fatigue endurance of EUROFER97 [14-17], but the number of tests performed is insufficient to stablish the design rules. Although, the literature on LCF behavior of EUROFER97 is good from materials science point of view, microstructural changes resulting from LCF and data to design is scarce. For that reason, a series of round-robin tests were launched under the framework of EUROfusion Program within the Engineering Design Data Integration (EDDI) Project. The aim of this work is to show the new low cycle fatigue results obtained on EUROFER97-2 at CIEMAT in comparison to previously done, together with the microstructural evolution developed during the test at different strain amplitudes.

3. EXPERIMENTAL PROCEDURE

The material used in this work is the EUROFER97-2 (9Cr-1WVTa) procured to the specification given elsewhere [18].The nominal chemical composition is given in Table 1. Low cycle fatigue (LCF) tests have been performed in air using round specimens (Fig. 1). Samples were machined and provided by The Karlsruhe Institute of Technology (KIT) on as-received condition; normalization at 980ºC/30'/air cooling plus tempering at 760ºC/90'/ air cooling.

Table 1: Chemical composition of EUROFER97-2 (wt. %)										
C	Cr	V	Ta	W	Ti	Mn	P	S	N_2	Fe
0.110	8.95	0.202	0.120	1.06	0.001	0.55	0.0010	0.001	0.022	Balance
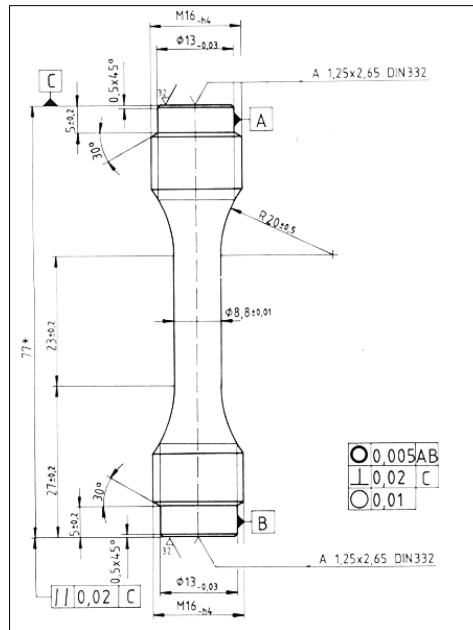
Fig. 1: Low Cycle fatigue specimen geometry.

Tests were conducted in air with a servo-hydraulic MTS 310 testing machine equipped with a radiant furnace. LCF was carried out under strain control with a triangular fully reversed wave shape, using high temperature axial extensometer of 25 mm length. The specimens were tested at room temperature and at 550 ºC with a constant strain rate of 3.10^{-3} s^{-1} and at 0.4, 0.6, 0.8, 1, 1.4 and 1.8 % total strain range. The temperature control

3

was performed using two independent PDI loops. Two different Type-K thermocouples were directly welded to the specimen to obtain the feedback temperature. The fatigue life, N_f, was determined as the number of cycles up to complete failure.

After the tests, the fracture surface was examined by stereoscopic microscope.

The microstructures of the specimens have been characterized on thin foils and carbon extraction replicas using transmission electron microscopy (TEM) and scanning TEM (STEM) techniques on a JEOL JEM 3000F equipped with an EDS detector. The STEM unit has an annular dark field detector (ADF) that makes possible to acquire both, low angle (LAADF) or high angle annular dark field (HAADF) images by changing the camera length. The characterization of microstructure has been mainly performed in STEM mode by acquiring LAADF images or –in some cases- HAADF images to remove contrast from forest dislocations and a purer Z-contrast of the precipitates in the images. TEM discs with 3 mm of diameter close to fracture surface along the load application direction, Fig. 2 were extracted and thinned using a Struers Tenupol-5 electropolishing unit with a methanol - sulfuric acid (4:1) solution at 10 V and at 15 °C. Only the discs closest to the crack were studied for this work.
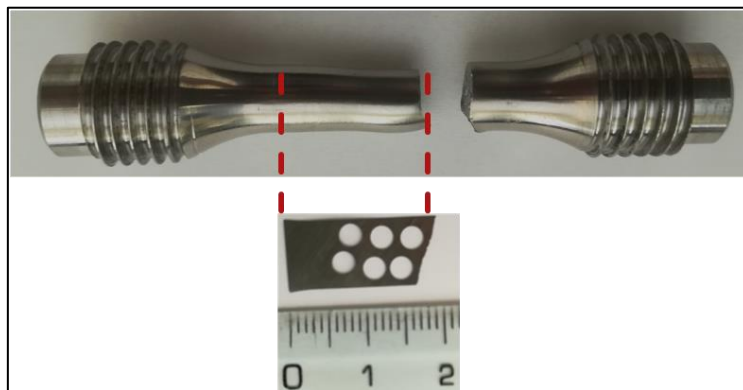
Fig. 2: Broken LCF specimen showing the place where the 3 mm discs were extracted.

4. RESULTS

4.1 Cyclic stress response

Regarding fatigue properties, Fig. 3 shows the total strain as a function of the fatigue life N_f, at room temperature and 550 °C. It has been added, for comparison, data

obtained under quite similar conditions (500 °C and strain rate of 5.10^{-3} s^{-1} on EUROFER97) [18]. As expected, the life of EUROFER97-2 under tension-compression cycled decreases at high temperature (550 °C). However, these differences on fatigue life are strongly dependent on the total strain range. As a general rule, high total strains (1.8 and 1.4 %) produce not significant reductions on fatigue life between room temperature and 550 °C, while for lower deformations (0.4 and 0.6%), the number of cycles to failure is reduced significantly [12, 19, 20].
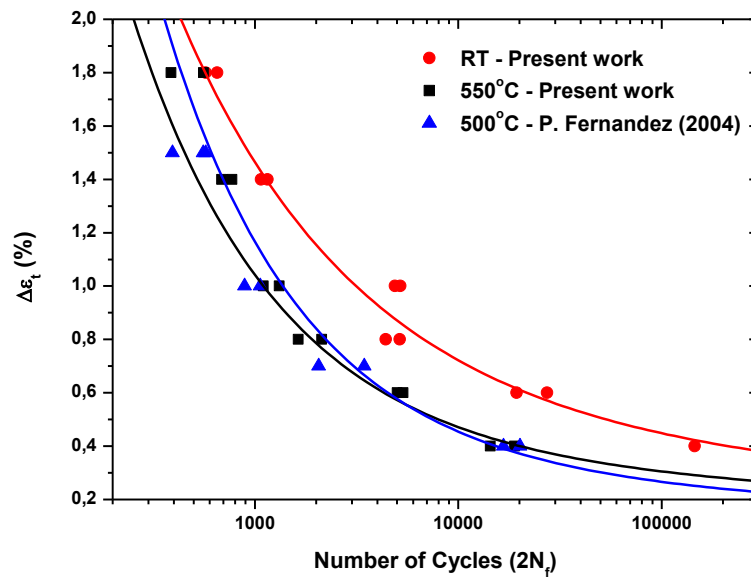
Fig. 3: S-N curves for EUROFER97-2. Red circles and squares in black point the values obtained in this work at room temperature and 550ºC respectively. Triangles in blue represent values at 500 ºC in EUROFER97 published in [18].

The peak stress evolution *vs.* the *number* of cycles for all total strain ranges is illustrated in Fig. 4. Stress values were acquired in each cycle. Room temperature curves indicate a short period of rapid hardening behavior which is similar to that previously observed in EUROFER97-2 by Marmy et al. [12] and in other different alloys like 9Cr-1Mo [21]. Despite this slight growth in the peak stress during the initial cycles it cannot be attribute a significant tension peak evolution capable of causing a continuous and significant hardening during a prolonged period of life of the material during the LCF test. In both cases, at 550 °C and at room temperature, after certain cycles a continuous softening until the failure has been measured.
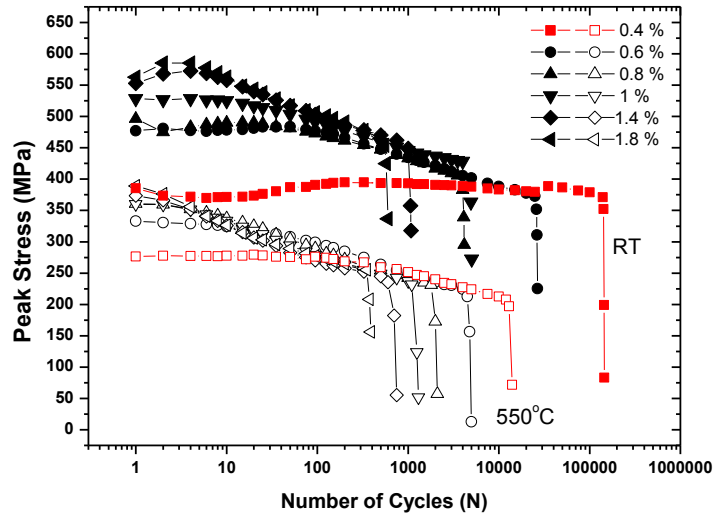
Fig. 4: Tension peak stress as a function of the number of cycle (N) up to failure, at room temperature and 550ºC and at 0.4, 0.6, 0.8, 1.0, 1.4, 1.8 % total strain. For simplicity, only a selected representative number of cycles have been plotted.

The results at room temperature and at 550 ºC have been evaluated according to the Coffin-Manson procedure [22, 23], taking into consideration total strain, $\Delta\varepsilon_t$, elastic and plastic strain range, $\Delta\varepsilon_e$ and $\Delta\varepsilon_p$, which are represented as a function of the cycle number (Fig. 5), the plastic and elastic values were calculated according to que following equation:

$$\Delta\varepsilon_p = \Delta\varepsilon_t - \Delta\varepsilon_e \quad \text{and} \quad \Delta\varepsilon_e = \sigma_{Nf/2} / E \tag{1}$$

Where $\sigma_{Nf/2}$ is total stress at half-life and E the elastic modulus.

6
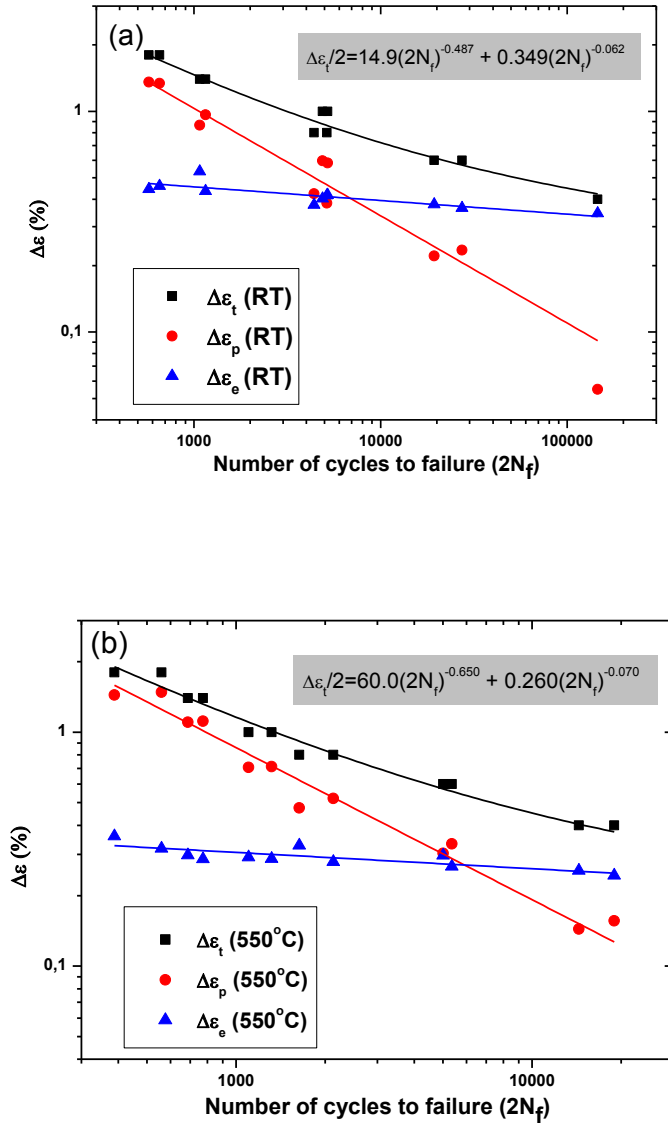
Fig. 5: *Total strain (Δε$_t$), plastic strain (Δε$_p$) and elastic strain (Δε$_e$) as a function of the number of cycles to rupture (a) at room temperature and (b) at 550 ºC .*

The Coffin-Manson equation allows the evaluation of the total strain as a function of the number of cycles following the form [24-26]:

$$\frac{\Delta\varepsilon_t}{2} = \frac{\Delta\varepsilon_e}{2} + \frac{\Delta\varepsilon_p}{2} = \frac{\sigma'_f}{E}(2N_f)^b + \varepsilon'_f(2N_f)^c \qquad (2)$$

where b, c, $\varepsilon_f^{'}$ and $\sigma_f^{'}$ are material constants.

Coffin-Mason exponent (c) is an indicator of life fatigue, which usually varies from -0.5 to -0.7 in similar alloys [27-31]. Calculated coefficients and exponents are summarized in Table 2. As expected, the exponent obtained for room temperature tests is smaller than the measured one at 550 ºC which implies that fatigue life is shorter at a higher temperature.

Table 2: Summary of values obtained in LCF tests					
	Basquin coefficient (σ_f' / E)	Basquin exponent (b)	Coffin-Manson coefficient (ε_f')	Coffin-Manson exponent (c)	Transition life in cycles $\Delta\varepsilon_p = \Delta\varepsilon_e$
RT	0.349 ±0.044	-0.062 ± 0.015	14.9 ± 4.3	-0.487 ± 0.041	6879
550 ºC	0.260 ± 0.036	-0.070 ± 0.017	60.0 ± 27.5	-0.650 ± 0.063	5908
500 ºC [18]	0.27	- 0.060	38.0	-0.62	-0.62

From Fig. 5 is also deduced that a total strain of 0.4 % has a very low plastic component at room temperature. The predominance of the elastic deformation causes de absence of softening as can been clearly observed in Fig. 4. The relationship between plastic strain component and softening can analytically parametrized using the cycling softening coefficient, S, calculated fitting, in the linear range of the curves in Fig. 4, following the expression:

$$\sigma = AN^{-S} \qquad (3)$$

Where σ is the peak stress, A a constant, N the number of cycles and the exponent S the cyclic softening coefficient. Fig. 6 shows S, and the plastic component percentage as a function of the total strain.
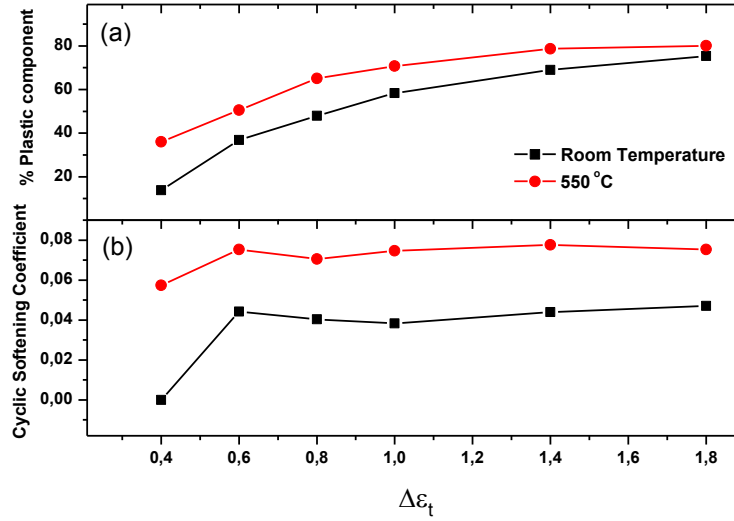
Fig. 6: (a) Plastic strain component percentage and (b) Cyclic Softening coefficient versus total strain.

As a confirmation of that observed in Fig. 5, plastic strain component continuously increases when total strain also increases and it is higher at high temperature which has been also observed by Armas et al. [32] and P. Marmy et al. [12] in EUROFER97. The softening is almost constant from 0.6 to 1.8 total strains for both studied temperatures and it significantly decreases, especially at room temperature, when total strain is 0.4 %.

4.2 FRACTURE SURFACE

Fracture surface was studied by means of a stereoscopic microscope because of the depth perception it provides. The analysis revealed that the fracture surface depends completely on the deformation amplitude, temperature and possible nucleation crack sites such as surface imperfection due to the fabrication process or microstructural characteristics as inclusions, hard precipitated particles or crystal discontinuities.

Fatigue cracks initiate and propagate in zones where the strain is most severe, usually structural defects. Due to the cycling loads, the region under plastic deformation develops at the defect tip, which will become an initiation site for a fatigue crack, propagating until specimen fracture. It is well known that fatigue consists in three stages well defined [33]: stage I, initiation of the crack (s), stage II, propagation or growth due to the cycling loads and stage III, fracture which normally is very fast, when the cross

section left cannot withstand the load. In all the analyzed surfaces, stage I zone was insufficiently defined in order to perform a deep characterization, on the contrary, stage II and III were very well defined. As expected, EUROFER97-2 is very resistant to oxidation so all the surfaces were smooth and well defined, hence all the features were easily detectable.

Specimen tested at RT and 0.4 % (Fig. 7 a) presented 2 cracks opposite each other which converged almost at the center of the specimen. It showed the typical striation marks produced in a completely ductile material with regular size and spacing. Increasing the test temperature (550 ℃) the circular striations were not observed, however, from the two crack nucleation sites detected, plenty of straight striations following the main crack growth direction were developed during the test, (Fig 7 b). These characteristics are most commonly seen when the material is completely ductile and its microstructure is formed mostly by one phase or contains a small fraction of other constituents, so there is practically no crack nucleation at second phase interfaces or even by cleavage in secondary phases.

At the intermediate strain range, 0.8 % and 1 % at RT (Fig 7 c and e) the fracture surface is practically identical (in fact the fatigue life results are very similar). In both surfaces shear lips ae observed, one quite pronounced in the specimen tested at 0.8 %. There are some ratchet marks among the initiation crack sites but no beach marks, at least clearly identifiable. However in the specimen at 1%, it is detected a small area containing curved beach marks nearby the initiation crack site (downside left). On the other hand the fracture surface at 550 ℃ is more different than the one at RT when comparing 0.8 and 1% strain range. At 0.8 % (Fig. 7 d) a clear shear lips are observed and beach curves surroundings the cracks initiation sites which seems to be produced by oxidation. The crack formed from the lower side seems to have propagated faster or the crack originated at the upper side was created later. At 1 % and 550 ℃ there is only one crack which crosses the entire surface. Typical beach curves following the typical ductile fracture surface up to fracture. Finally the fracture surface originated when the deformation is 1.8 % at RT (Fig 7 g) presented circular striations but less depth is reached, starting the ductile fracture zone before than the specimen at 550 ℃ in which the striations appeared at the center of the specimen. In the surface of the aforementioned specimen, several main cracks were detected with at least 4 clear

terminals shear fractures. Each plateau produced very short spaced striations, indicating that the plasticity at 550 ºC of EUROFER97-2 increases with temperature, Fig. 7 h.
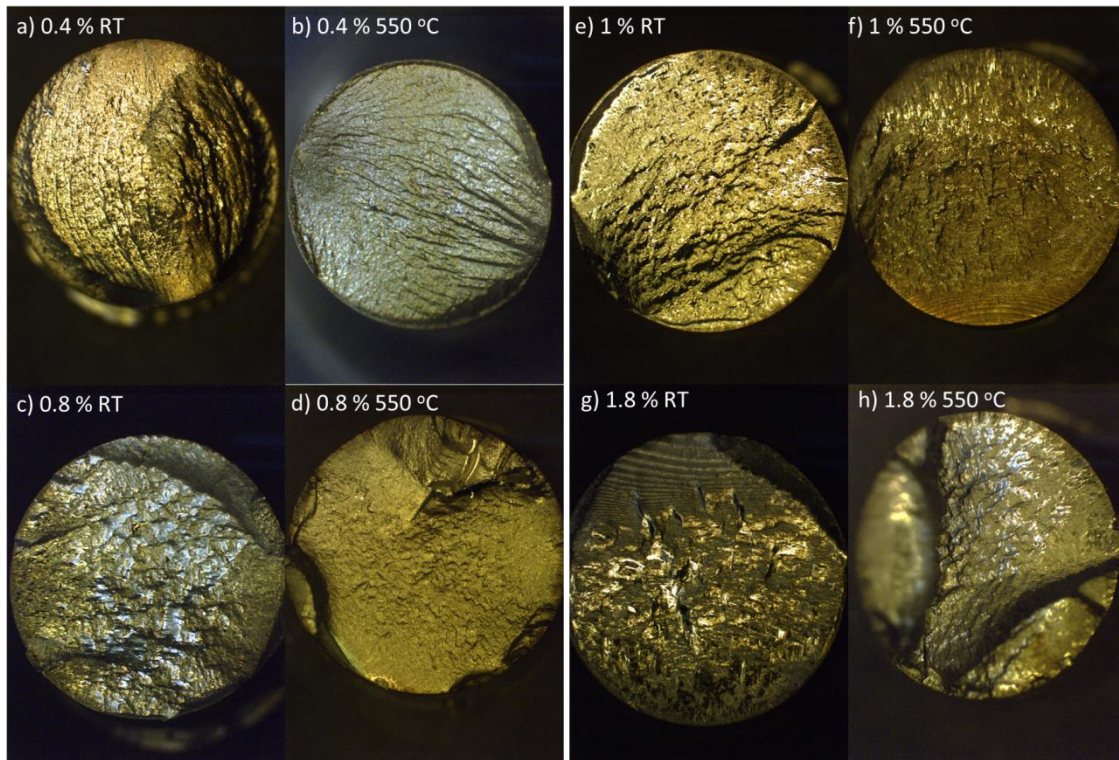
Fig. 7: Fracture surface of EUROFER97-2 resulting at a) 0.4 % - RT, b) 0.4% - 550 ºC, c) 0.8% - RT and d) 0.8 % - 550 ºC, e) 1 % - RT, f) 1% - 550 ºC, g) 1.8% - RT and h) 1.8 % - 550 ºC.

5. MICROSTRUCTURE CHARACTERIZATION.

5.1 AS RECEIVED MICROSTRUCTURE.

EUROFER97-2 exhibits principally martensite structure on as received condition. The detailed examination of this version of EUROFER97-2 revealed some microstructural differences with respect to the widely studied EUROFER97-1[34] which is fully martensitic. The Alloy used in this work, presented a few ferrite grains, Fig. 8, along with some areas with a very high dislocation density which remains after tempering. The identification of the microstructure below is difficult even using STEM detector as shown in Fig. 9, which makes harder the width lath counting since it is an important parameter to take into consideration when fatigue life is studied [35] (in fact, smaller PAG which implies smaller lath size normally improves fatigue properties [36]). Although it is expected that these high dislocation density zones are martensitic

11

structure, since in RAFM steels with some ferrite grains, only the martensitic laths contain the most dislocations by comparison to ferrite structure, as observed by Fernández et al. [37]. Additionally, it was observed some laths free or with a lower amount of dislocations along with zones with the aforementioned distorted structure. The prior austenite grains (PAG) are subdivided into packets, blocks of laths and sub-grains along the laths (Fig. 8). A packet is a region which consists of parallel laths with the same habit planes, however, they can be misorientated between one another, or even have different orientations. Nevertheless, the laths in a block are parallel with the same orientation and/or misorientations smaller than 5º. The angle between these microstructural features has been proved to have a clear influence on microstructural evolution during LCF [35, 38].
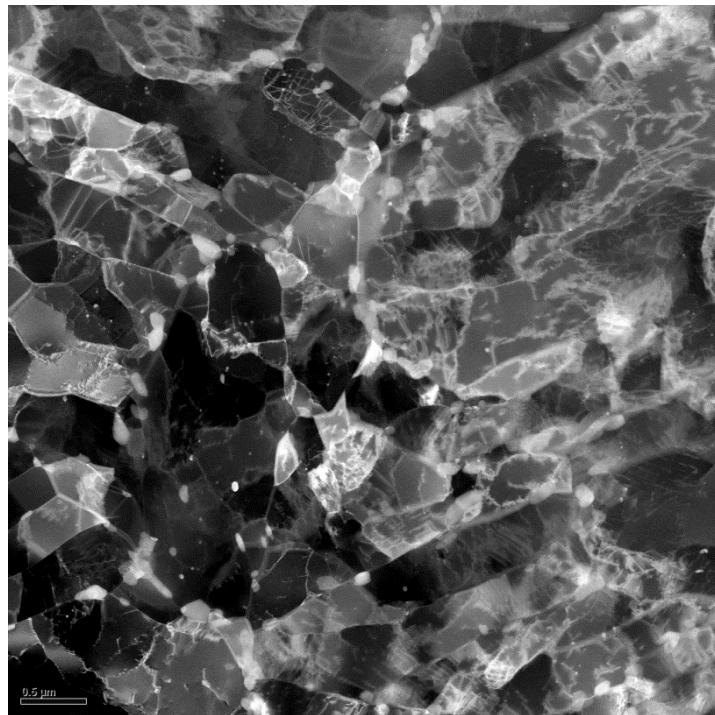
Fig. 8: STEM image of EUROFER)/-2 on as received state (normalization at 980ºC/30'/air cooling plus tempering at 760ºC/90'/ air cooling) showing many ferrite grains along with some martensite laths.
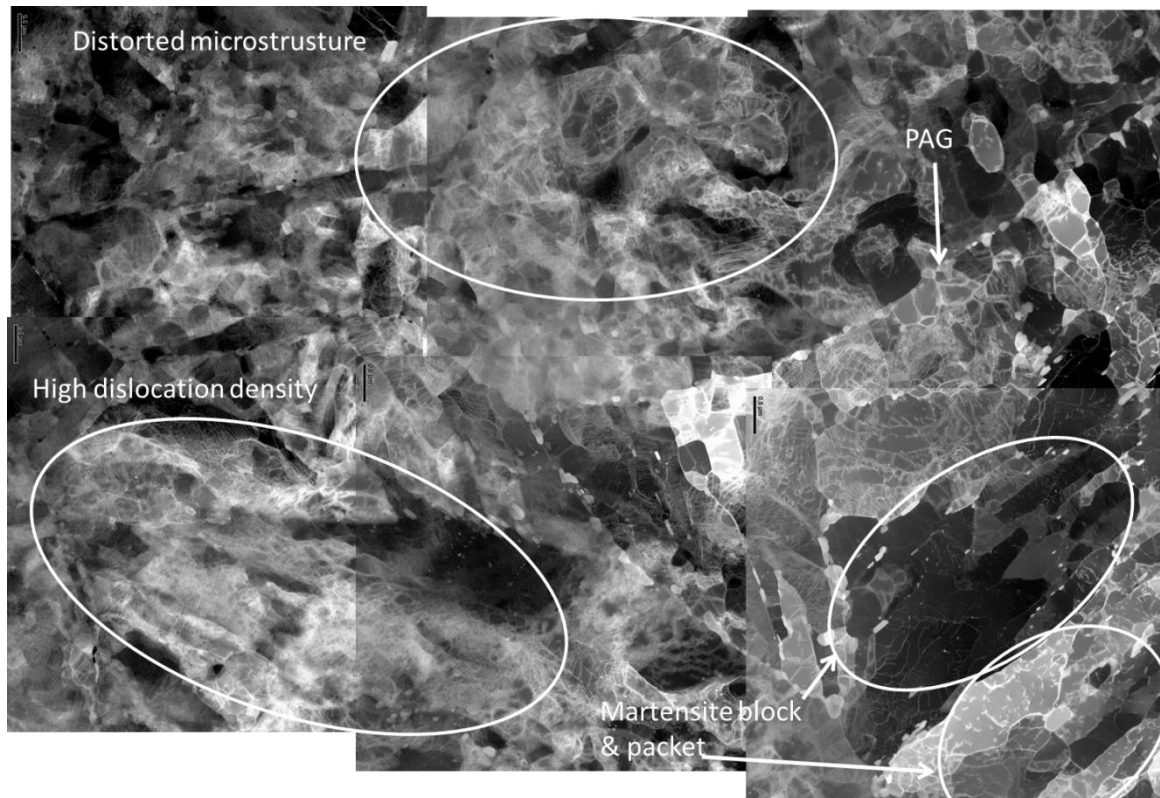
Fig. 9: STEM image of EUROFER97-2 after normalization at 980ºC/30'/air cooling plus tempering at 760ºC/90'/ air cooling (as received state).

Secondary phases precipitated after tempering are shown in Fig. 10, which is a micrograph obtained by means of an HAADF detector in STEM microscope. According to the study on carbon extraction replica (described below) the most abundant are Cr-rich carbide of $M_{23}C_6$ type. These carbides are mainly precipitated on PAG and martensite laths, and to a lesser extent even inside the laths.

However, the same coarse carbides were detected along subgrains boundaries, identifying in some cases a clear agglomeration. In addition, finer precipitates of type MX (V and Ta rich) were detected principally precipitated inside the martensite laths
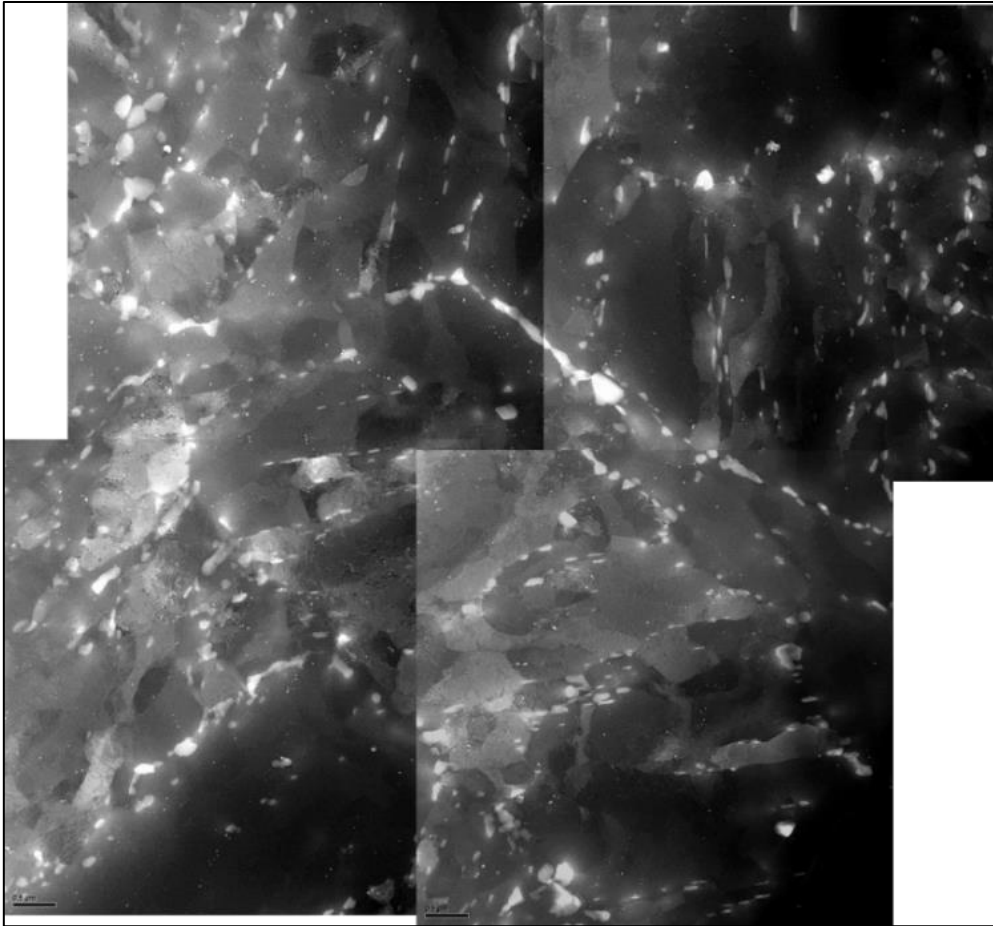
Fig. 10: STEM HAADF image composition showing the precipitation of secondary phases after tempering of EUROFER97-2.

Particle composition, size and distribution are key microstructural features to take into account to evaluate the microstructural development when either static or cyclic loads are applied as in the present investigation, trying to detect any possible synergy between strain and temperature regarding particle growth. For that, carbon extraction replicas were fabricated to determine the characteristics of secondary phases.

The identification and microchemistry of the secondary phases was performed on carbon extraction replica to avoid matrix effects. Two types of precipitates were tentatively identified by EDS (Fig. 11); Cr-rich carbide ($M_{23}C_6$) and MX (V-rich and Ta-rich), which are the same kind that the identified on EUROFER97 [34]. The majority and coarser phase was the $M_{23}C_6$ (whose size was from 64 to 278 nm) and the finer particles (with a size range from 11 to 53 nm) were the carbo-nitrides of MX type .The microchemistry of secondary phases after tempering on EUROFER97-2 is presented in Table 3.
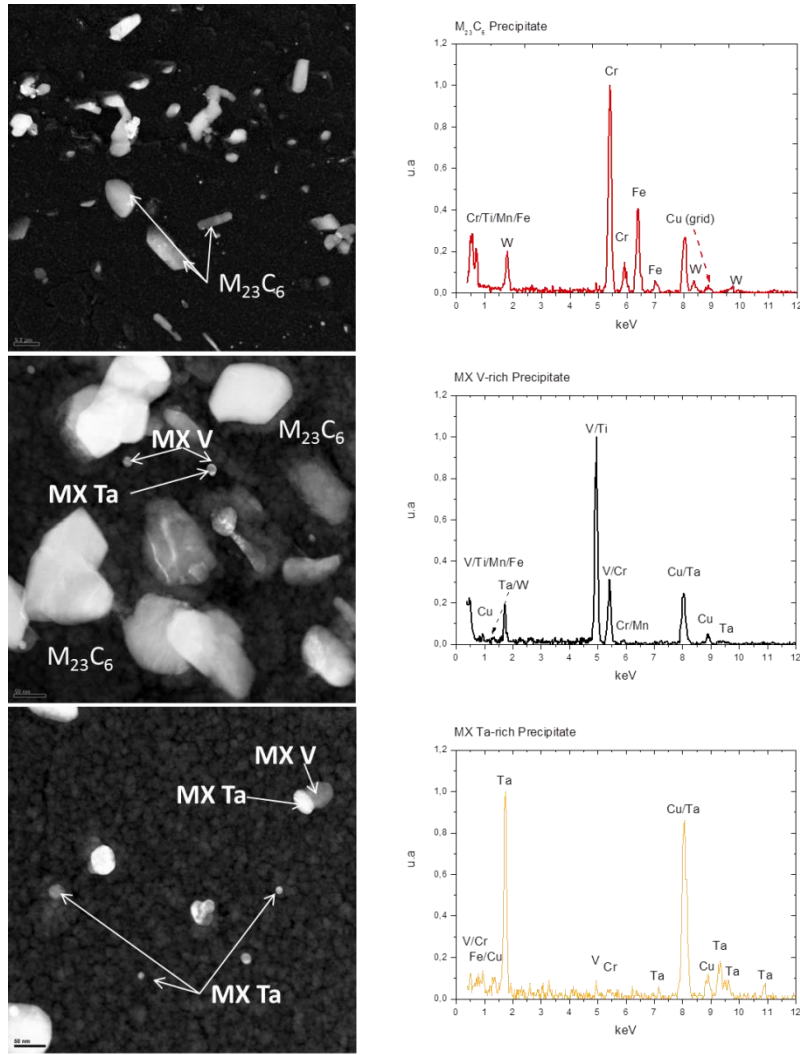
Fig. 11: STEM micrographs of carbon extraction replica of EUROFER97-2 in as received state, along with typical EDS of $M_{23}C_6$ (up), MX V-rich (center) and MX Ta-rich (down).

Table 2: Chemical Composition of precipitates studied in the carbon extraction replica (at. %).								
	Fe	**Cr**	**W**	**V**	**Ta**	**Mn**	**Ti**	**Average size [nm]**
$M_{23}C_6$	27.4 ± 2.1	66.0 ± 2.0	4.1 ± 0.8	0.4 ± 0.2		2.3 ± 1.0	0.3 ± 0.1	167 ± 100
MX Ta rich	1.7 ± 0.4	5.6 ± 2.0	3.8 ± 2.6	10.7 ± 5.0	77.8 ± 4.7	0.6 ± 0.4	1.4 ± 0.4	19 ± 8
MX V rich	0.4 ± 0.1	13.6 ± 0.7	1.08	81.5 ± 2.6	3.6 ± 2.6	1.0 ± 0.2	0.9 ± 0.7	48 ± 9

Carbon extraction replicas were extracted from 3 different areas in order to evaluate the distribution of precipitates exhaustively. As reference, the precipitation of 3 STEM micrograph compositions were counted as can be seen in Fig.12. Every composition corresponds to a different population density: 2526, 2187 and 1296 precipitates were found on Fig.12 a), b) and c) respectively. In addition, Fig. 13 shows the size distribution of the precipitates observed in Fig 12, including as well, an average

population density calculated with all the previous results. The study on as-received state revealed a very heterogeneous distribution of precipitates. However the largest amount of precipitate size is lower than 50 nm, which may correspond with MX-type. These observations make difficult the study to the precipitates evolution (distribution, growth, agglomeration…) during LCF and consequently its effects on fatigue life.
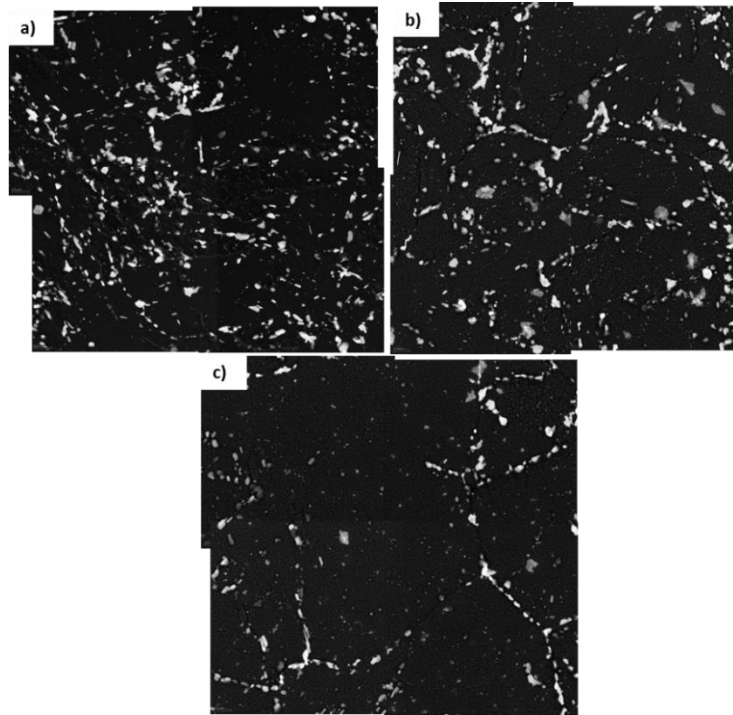
Fig. 12: STEM micrographs of carbon extraction replica of EUROFER97-2 in the as received state, showing the heterogeneous distribution of secondary phases.
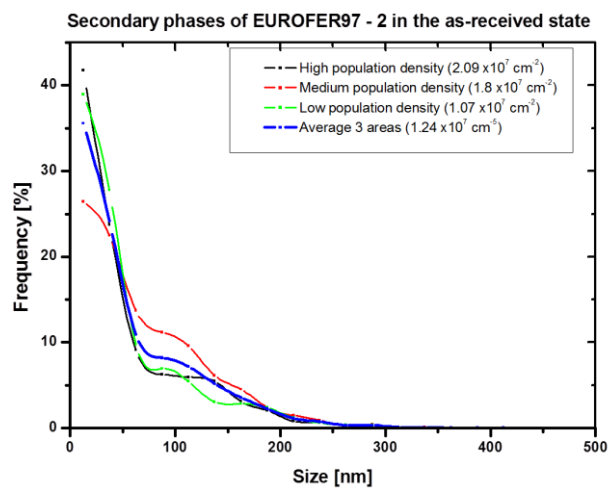
Fig. 13: Secondary phase sizes distribution of EUROFER97-2 in as received state (N +T)

5.2 MICROSTRUCTURAL DEVELOPMENT UNDER STRAIN

The microstructural characterization was performed on the following total strains: 0.4 0.8, 1 and 1.8 %. These strain values correspond to the studied lowest, intermediate and highest total strains which illustrated the whole microstructural evolution of EUROFER97-2 of the entire strain range.

The EUROFER97-2 after cycling at 0.4 % presents slight microstructural changes with respect to the as-received state. The density of dislocations, in general, appears to decrease in comparison to that un-deformed state (Fig. 8), but with clear differences between grains. High dislocation density within the martensite laths is still present (Fig. 14 a). However, sub-grains with very low dislocation density and scarce precipitation inside of them were also found as highlighted in a red circle on the aforementioned figure. Probably, these grains have been formed during cyclic straining as consequence the dislocations glide freely (low density of particles to pin the dislocations) through the martensite sub-grain and the dislocation reactions at sub-grain boundaries leading to martensite laths break-up and sub-grain formation. As the strain range level increase up to 1% practically all the original martensite developed into ferrite grains (Fig. 14 b and c). Only a very few traces of the original laths were observed. The most relevant differences between 0.8 and 1 % strain amplitudes are concerning the significant growth of the sub-grains at 1% (Fig. 14 c).

Finally, the resultant microstructure after the cycling at 1.8 % and RT is more complex than in the other strains (Fig. 14 d). The microstructural changes developed after cycling have produced a mixture of some original martensite laths, pronounced sub-grain formation with trace and shape of martensite laths and well developed ferrite grains (as highlighted with red circles). Independently of the grade of transformation of martensite, the overall reduction of dislocation density is significant in comparison with the as-received state, maintaining the lath structure, but as mentioned with a clear reduction of dislocation density within the new fully developed grains and former martensite sub-grains. Nevertheless, most of dislocations seem to be annihilated within the grains and accumulated at the grains boundaries, as seen in Fig. 15. Comparing all the resultant microstructures at RT (0.4, 0.8, 1 and 1.8 %), it proves that the EUROFER97-2 seems to be able to accommodate plastic strains per cycle up to strain amplitudes of 1%, leading to a microstructural development based mainly on partial or

total elimination the original martensite structure as consequence of the mobility and annihilation of the dislocations. However, increasing the strain amplitude up to 1.8% the EUROFER97-2 seems not to be able to accommodate the large plastic strain, producing rapid softening and consequently failure.
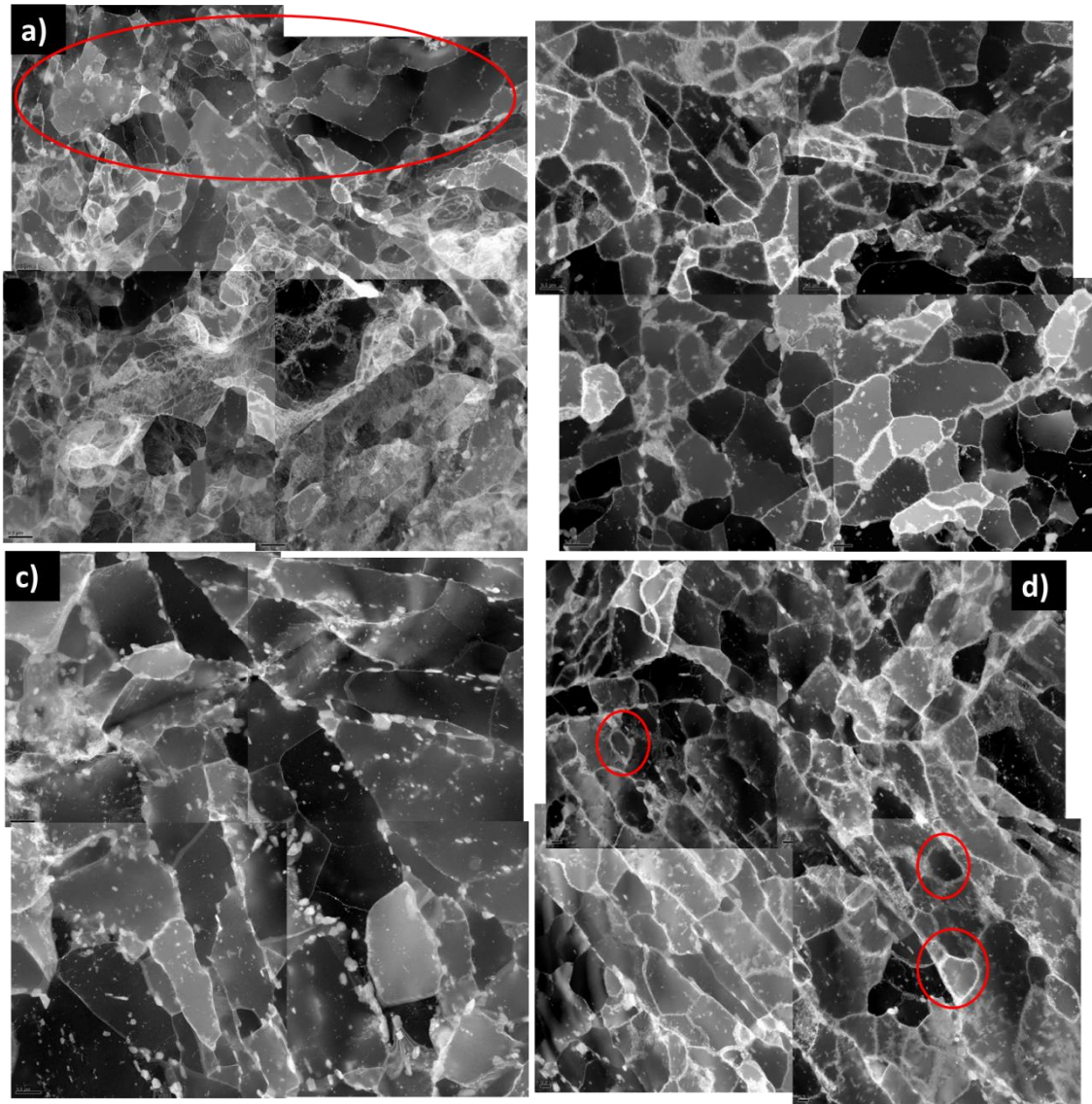
Fig. 14: Representative microstructure obtained by STEM of samples fatigued at room temperature and a strain range of a) 0.4 %, b) 0.8 %, c) 1% and d) 1.8 % up to rupture.
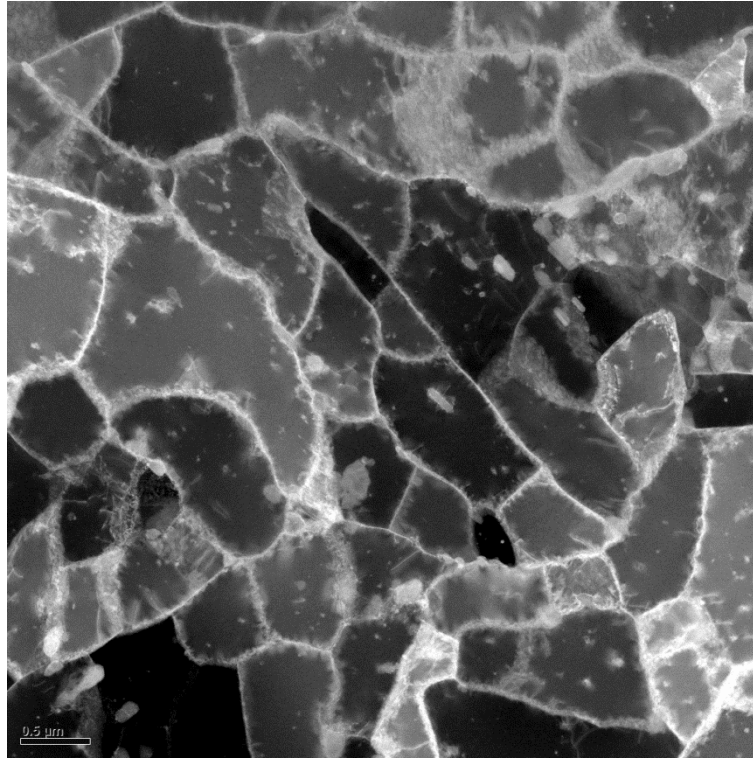
Fig. 15: Dislocations accumulated at the boundaries on EUROFER97-2 tested at 1.8 % and RT.

After the test at 550 ℃ and 0.4% total strain, the microstructure is completely different (Fig. 16 a) in comparison with the microstructure developed at room temperature Fig. 14 a). Practically all the lath and subgrain microstructure has transformed into a large equiaxed ferrite grains. Only a few sub-grains fragmentation with trace of original martensite laths was detected. The boundaries of these fragmented sub-grains are decorated with secondary phases which their density and distribution that seem to the ability of pinned the boundaries and to avoid the coarsening of sub-grains. The majority of secondary phases due to the motion of the boundaries are confined inside of ferrite grains, drawing the original martensite laths and sub-grain boundaries. Regarding dislocation density, the large ferrite grains developed during the cyclic straining are practically clean of dislocations. Most of dislocation density was observed in the fragmented sub-grains of martensite laths.

At 550 ℃ and strain amplitudes of 0.8 % (Fig. 16 b) the coarsest grains present polygonal morphology, suggesting that the sub-grain formation occurs in two steps; firstly by the widening of the martensite laths and second by the break-up the sub-grains. Contrary at 1 %, the microstructure is less affected than at lower strain ranges (Fig. 16 c). Partially eliminated original sub-grains, grain growth and rearrangement of

dislocations at boundaries are evident. These unexpected microstructural findings could be due to the fact that the area of the observation of the TEM disc could correspond to the zones of the material with very high dislocation density and/or distorted areas as the identified in Fig. 9.

On the other hand, after 1.8% and 550 ºC (Fig. 16 d) practically all the original martensite laths have evolved into large new grains with high dislocation density at their walls. However, due to the high density of precipitation density found in the analyzed areas, dislocation networks along with isolated linear dislocations were observed pinned to secondary phases avoiding the gliding to the boundaries (some examples are highlighted with red circles in Fig. 16 d).
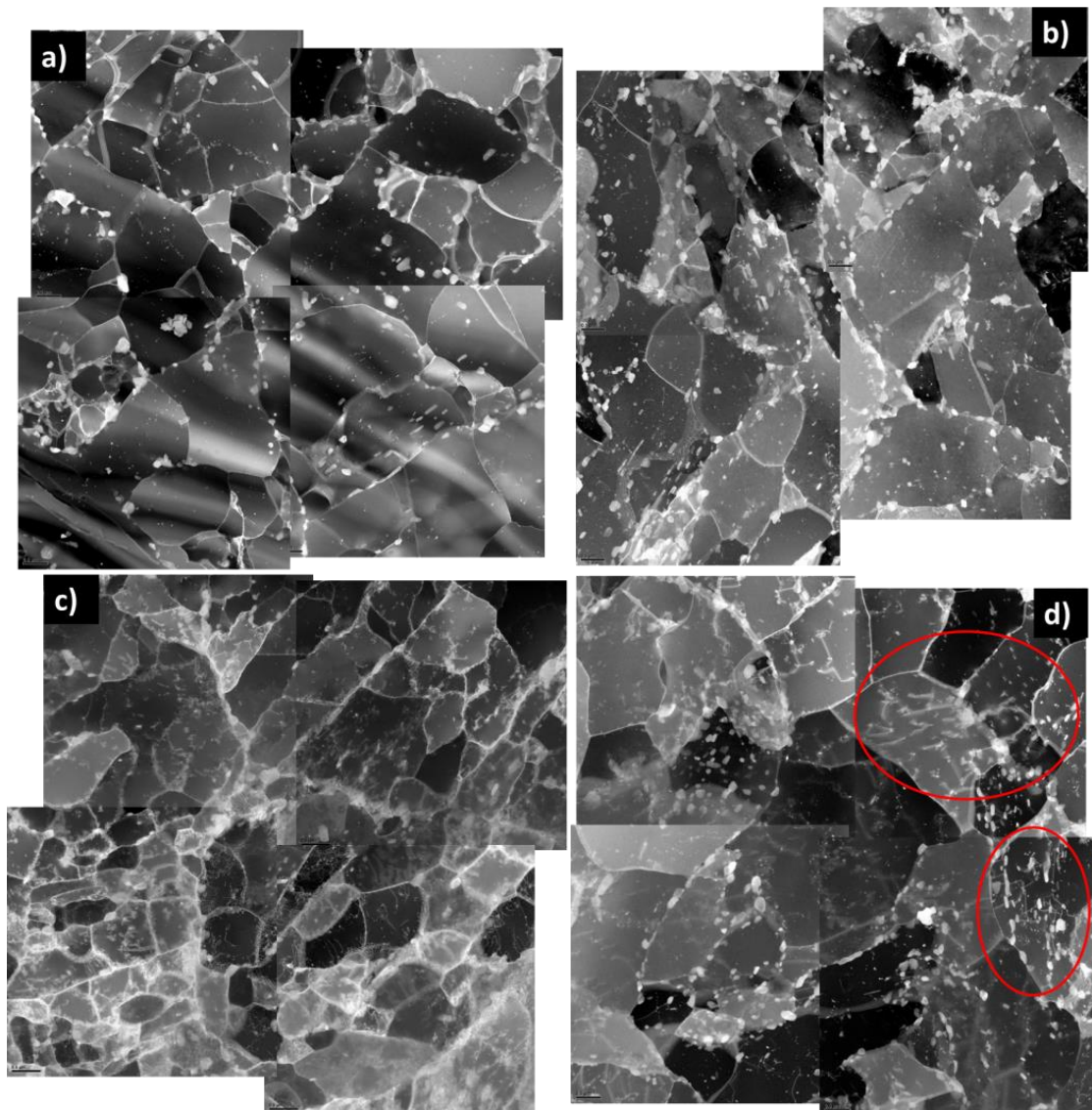
Fig. 16: Characteristic microstructure obtained by STEM of samples fatigued at 550 ºC and a strain range of a) 0.4 %, b) 0.8 %, c) 1% and d) 1.8 % up to rupture.

Regarding secondary phases, carbon extraction replicas from each test condition of 0.4, 0.8, 1 and 1.8 % at RT and 550 ºC respectively were studied by STEM, and compared to the extracted ones in the as received condition, in order to evaluate the influence of strain range and test temperature on secondary phase evolution. It is important to remark that the EUROFER97-2 exhibit very heterogeneous particle distribution independently the precipitate kind (MX or $M_{23}C_6$), as showed previously. The number of particles differs from one zone to another in the same TEM disc, as shown in Fig. 12, but the size distribution kept in average constant, as depicted in Fig. 13. Nevertheless, to extract if there is any possible type of synergy between temperature and strain, precipitates were studied by STEM (Fig. 17) and statistically treated as shown below.
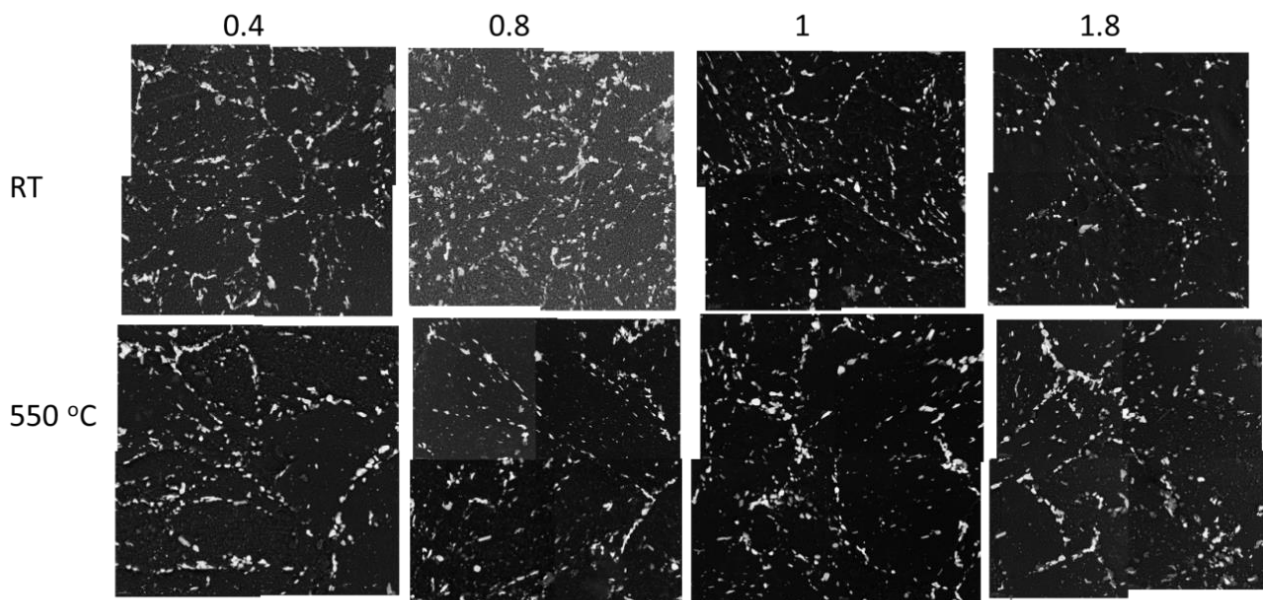
Fig. 17: STEM carbon extraction replica micrograph comparing secondary phase evolution in as after LCF tests at different conditions (0.4 %, 0.8%, 1%, 1.8 % at RT and 550 ºC respectively).

Size and amount of secondary phases were determined taken an area of around 120 μm^2 (Fig. 17) for each specimen. Those results were depicted in Fig. 18, where not clear synergistic effect can be extracted from between strain range and test temperature. In addition, the heterogeneous distribution was observed again, since for 1.8 % at 550 ºC and RT were counted 2028 and 762 precipitates respectively for the same area. These results can be misinterpreted if analyzed them isolated, because it may be misled a possible increase of precipitation. However, comparing the as received results on

precipitation with the previous extraction replica observations, the variations can be addressed to a random effect due to the heterogeneous distribution of the material in the as-received state.
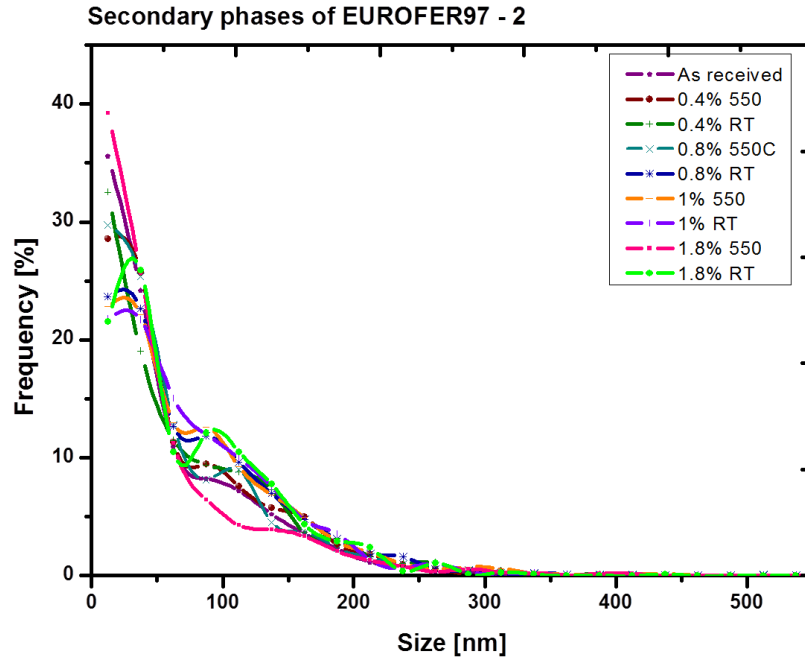
Fig. 18: Size distribution of secondary phases of EUROFER97-2 in as received state and after tested at 0.4%, 0.8%, 1% and 1.8% at RT and 550 ºC.

6. DISCUSSION

The new low cycle fatigue data obtained in this work, in order to stablish the mechanical rules for DEMO design, has confirmed the fatigue endurance of EUROFER97. This trend of behavior under cyclic testing was obtained in the past at both high and room temperature, although with a small differences manly due to the specimen geometry and environment conditions used during the tests (air or vacuum). In fact, a probe of so is depicted in Fig. 3 where the results of EUROFER97-1 obtained by P. Fernandez in 2004 [18] are included and the results are completely consistent. It is well known that fatigue tests are very sensitive to experimental parameters not only environment conditions [39], but also specimen size, strain rate or testing machine. In fact, in the literature there are similar results for the first version of EUROFER97, as Marmy et al.[12]. They also tested cylindrical plane specimens at 2.10^{-3} s^{-1} at room temperature and in the rage of 150 to 550ºC in vaccum. Marmy's results in fatigue life

22

are equivalent from those ones presented in this work[1] at room temperature. The calculated softening factors are quite close to the one obtained for us in EUROFER97-2 at 550 ºC which also is in good agreement with the value measured by Armas et al. [40] for F82H and MANET II for EUROFER97. In addition, Marmy probes that S it is independent of the strain rate (in the range 0.8 to 0.5%). On the other hand, Giordana et al. [41] showed that the softening evolution for lower plastic strains, 0.2 % at RT and 550 ºC and after an initial big drop, the stress remains constant. Despite different experimental conditions make it no directly comparable, softening seems trending to zero when strain also decreases below 0.5%. The calculated softening parameter, S, is practically null for this total strain, which shows a good agreement between the results in EUROFER97 and the present EUROFER97-2 data. Finally, Materna-Morris et al. [42] tested EUROFER97 in as received condition using small rounded specimens from a wide range of strains (0.4 to 1 %), and the results matches completely, as well. At lower strains there is almost no softening, and as increasing the strain, an instant hardening is showed at 1% before the stress drops, showing a clear softening. In the case of EUROFER97-2 under the specific experimental characteristics, the instant hardening is only observed at 1.4 and 1.8 %. Low softening is an indicator of low plasticity effects, as can also be observed comparing Fig. 6 a) and b). Since plastic deformation is related with non-reversible processes, its minimization is desired in order to increase life time of structural components.

Regarding microstructure to improve LCF life, a grain refinement is usually required. However, due to the complex and heterogeneous microstructure of EUROFER97-2 described in the previous paragraph interlath spacing may become important [43]. Although, it is possible the zones with non-defined structure affects the average LCF resistance, since remains to tangled boundaries formed by an agglomeration of dislocations. It has been observed that normally a reduction of PAG size leads a decrease of block and packet size, which means an increase of number of barriers to dislocation movement during deformation of lath martensite. This characteristic affects directly the strengthening of the material [44, 45], as well as, possible ferrite grains

---

[1] The authors appreciate that 'Cycle to failure' axes Fig. 5 in [12] may have to rescale in a factor 10 due an involuntary error in the preparation of the paper

which did not transform into martensite which have proved to be a more suitable phase to induce cracking [43].

On the other hand the effect of chemical composition is critical, since many authors have stablished that modifying the amount of W and Ta may alter the cyclic life, since those elements influence the size and distribution of the secondary phases precipitation (precipitation hardening) along with solid solution hardening. LCF life is closely related to material ductility, and therefore increasing W or Ta could be positive, but within limits because the larger the W-precipitates are, the higher loss of solid solution strengthened will be, so the material is more ductile.

The longest test at high temperature lasted 24 h, so in order to analyze how the temperature effects on the microstructure, an ageing of 24 h was performed on the as received material (tempered + normalize EUROFER-2) at 550 ℃. The resultant microstructure shows no changes regarding lath sizes, unresolved microstructure with very high dislocation density and some ferrite grains as shown in Fig. 19. Regarding secondary phase distribution in comparison with the as received material the results were almost the same, Fig. 20. Very heterogeneous distribution of precipitates with no shows of growth, or at least not detectable. In summary, these observations were expected, since in previous experiment, similar microstructural stability has been reported on normalized and tempered 9-12% Cr during subsequent annealing times up to 1100 h at 550 ℃ [46]. On CLAM martensitic steels [47] was observed an increase on martensite lath with for 2000 h at 500 ℃ but no sub-grain formation. On the other hand, for longer experiments as reported P. Fernández [48] on RAFM steels as EUROFER97-1 and F82H-mod up to 5000 h at 600 ℃ no microstructural changes were observed. Only when ageing tests are longer, 10000h, EUROFER97-1 at 500 ℃ showed some sub-grain equiaxed structure replacing the typical lath structure characterized with low or even none dislocations within. Lath coarsening is a phase transformation driven by dislocation movement with its following annihilation. Increasing temperature and time, the aforementioned transformation is enhanced. Although from a qualitative point of view, a slight dislocation reduction was observed in some grains, especially near the PAG boundaries. Some of them, appeared to be clean or with very few small dislocations (either in form of cells or isolated) pinned to small precipitates as seen in Fig. 21 (a – b). Thermal activated dislocation glided along the crystal with low carbides density up to grain boundaries forming knitting out cells as proposed [49].
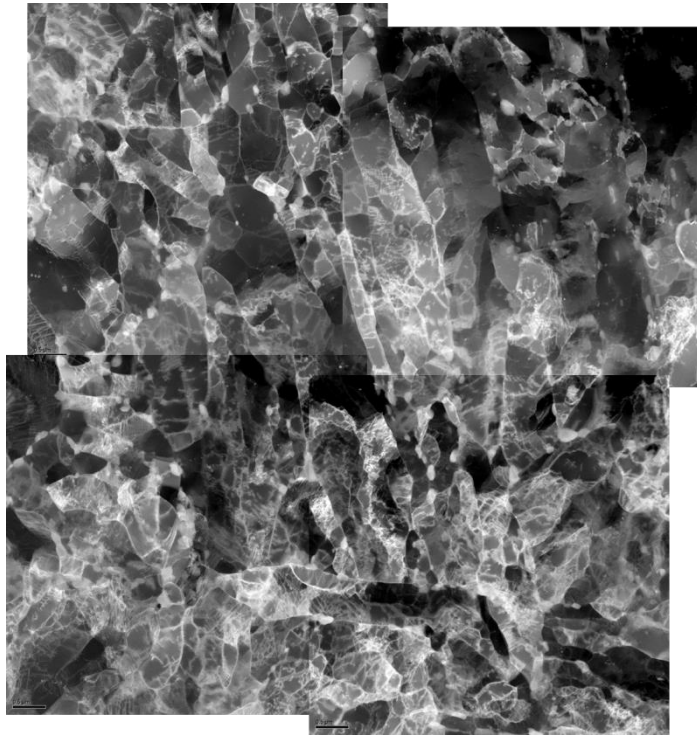
Fig. 19: STEM micrographs of the 24 h aged at 550 ºC of EUROFER97-2.
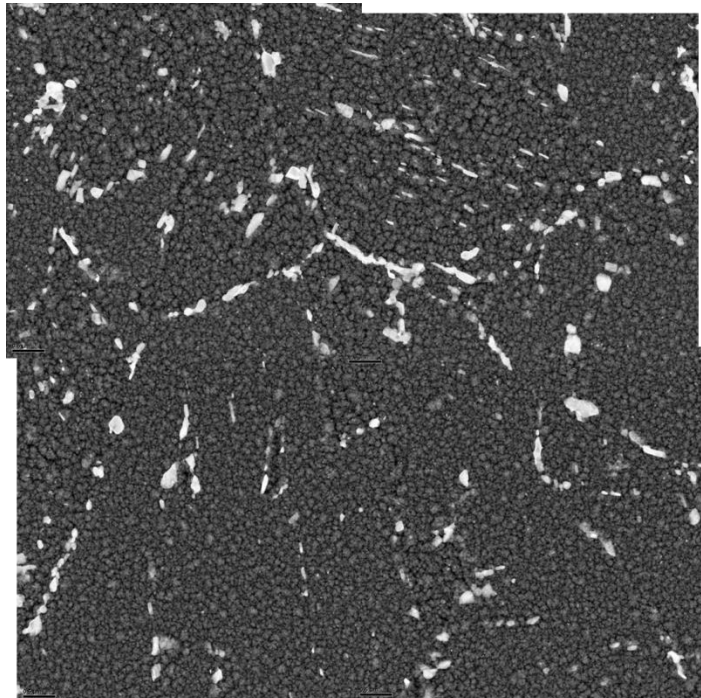
Fig. 20: STEM micrographs of carbon extraction replica of 24 h aged EUROFER97-2 at 550 ºC.
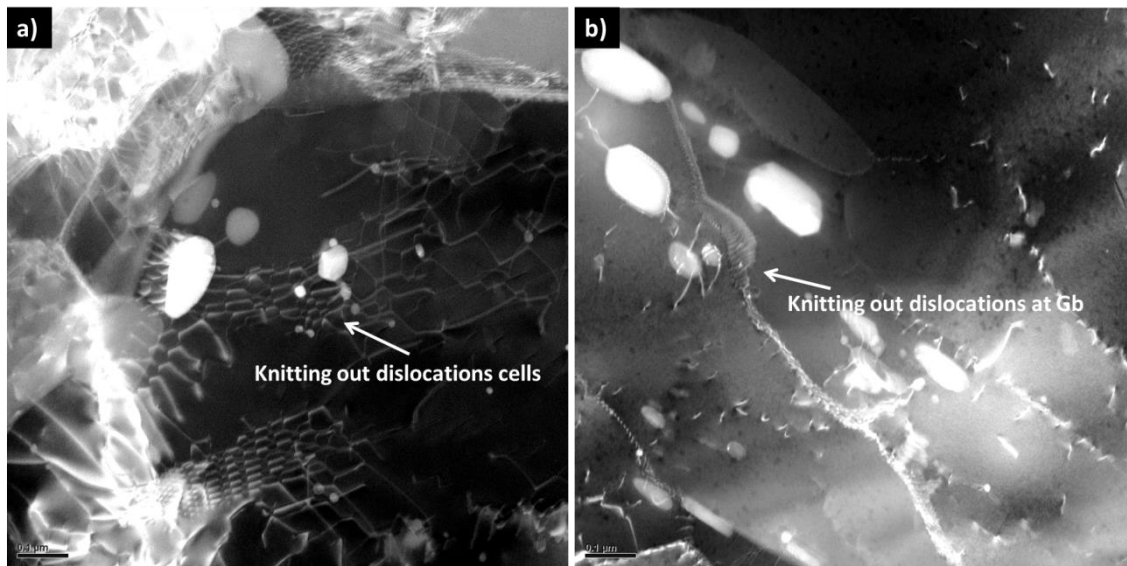
Fig. 21: STEM micrographs of particles pinning dislocations in form of cells from EUROFER97-2 aged 24h at 550ºC.

The apparent stability observed during ageing, martensite laths which are quite stable, could be destabilized under cyclic strain conditions as shown in literature in 9 Cr martensitic steels since its typical lath structure can be replaced gradually by a cell structure when fatigue experiments are performed [19, 50, 51]. Cottrell et al. [52] proposed that the behavior of the internal stress is the result of an interaction of strong athermal obstacles to the dislocation movement. Therefore, it can be concluded that these steels became weaker during cycling due to long range obstacles. Various mechanisms have been proposed to explain the cyclic softening [32] where two of them may fit at the beginning to the microstructural behavior observed in EUROFER97-2: On one hand, over-ageing which produces spheroidization and growth of the suitable secondary phases which, in turn, it worsen their distribution within the matrix. And, on the other hand, the transformation of martensite microstructure into subgrains with significant lower internal stress.

Carbides found along lath boundaries or PAG cause dislocation pinning effect [53-55], but the possible coarsening and spheroidization of those precipitates, as observed by Armas et al. [40] in EUROFER97 at 450 ºC, diminishes the role of $M_{23}C_6$ carbides as stabilizers of the subgrain microstructure, whose transformation is accelerated by cyclic strain, even more at high temperature. It is well known that those carbides including the smallest ones as V(C,N), Ta(C,N) and a combination of the aforementioned provided

stability to the martensitic structure at high temperatures [56] when the distribution is homogenous within the matrix.

It has been demonstrated that the final microstructure after LCF experiments depends on temperature and the strain amplitude, and the role of the dislocations is critical in the evolution of the microstructure. Golansky et al. [28, 51] proposed that at high temperature move due mostly to climbing of dislocation, since have enough energy to move out its plane, whereas at room temperature is driven by cross slip because the diffusion is low and difficult. The cyclic strain promotes the creation of point defects which is used for dislocation to move. In addition, the increase of dislocation density around precipitates observed in the micrographs showed previously can be an indicative of the participation of Orowan mechanism, when the dislocations try to skip those barriers, Fig. 21. In a quantitative point of view, there is not clear increase of size of the largest precipitates, as well as a promoting of agglomeration, especially at higher temperatures when the diffusion of substitutional elements is enhanced.

7. CONCLUSIONS

New LCF test and subsequent microstructural analysis in EUROFER97-2 have been performed in air at room temperature and 550ºC. Since there are not previous data for this EUROFER version, fatigue life, softening and Coffin-Mason parameters have been compared with data in the literature of the first version of EUROFER97 with a good agreement. Small differences can be attributed to variations in the experimental setup and test parameters. As a main conclusion EUROFER97-2 presents higher LCF life at room temperature and low strain. Both plasticity and softening behavior also decreases at lower total strain becoming negligible below 0.4% total strain.

At room temperature and low strain rate, the material microstructure remains very similar to the as received conditions, but showing some new ferrite grains with no dislocations within. As strain range increases, the increase of those grains are much clear up to the highest strain range, where the martensite lath shape is maintained but a clear widening of subgrains.

At 0.4 % and 550 ºC practically all the lath and subgrain microstructure has transformed into a large equiaxed ferrite grains. At 0.8 % the observations suggest that there are two clear steps of microstructural developing at high temperature. In the first place the widening of the martensite laths is produced, and afterwards, the breaking-up of the

sub-grains leading to rupture. However, at 1.8 % the microstructure is completely developed into new dislocation-free ferrite grains.

EUROFER97-2 secondary phases seem to be very resistant to change in terms of size and distribution under these cyclic testing conditions, although the material in the as received state showed large heterogeneous distribution of particles.

8. ACKNOWLEDGEMENT

9. REFERENCES

1. ASME, *BPVC Section III-Rules for Constructions of Nuclear Facility Components-Subsection NCA-General Requirements for Division 1* 2017.
2. Organization, I., *Structural Design Criteria In-Vessel Components (SDC-IC), IDM 222HC.* 2012.
3. AFCEN, *Design and Construction Rules for Mechanical components of FBR nuclear islands: RCC-MR*. Vol. A. 2007: AFCEN.
4. AFCEN, *Code of Design and Construction Rules for Mechanical Component in Nuclear Installations (RCC-MRx)*. 2013.
5. Porton, M., et al., *Structural Design Criteria Development Needs for a European DEMO.* Fusion Science and Technology, 2014. **66**(1): p. 18-27.
6. Ricapito, I., et al., *Technologies and modelling issues for tritium processing in the European Test Blanket Systems and perspectives for DEMO.* Fusion Engineering and Design, 2014. **89**(7-8): p. 1469-1475.
7. Aiello, G., et al., *Assessment of design limits and criteria requirements for Eurofer structures in TBM components.* Journal of Nuclear Materials, 2011. **414**(1): p. 53-68.
8. Zmitko, M., et al., *The European ITER Test Blanket Modules: EUROFER97 material and TBM's fabrication technologies development and qualification.* Fusion Engineering and Design, 2017. **124**: p. 767-773.
9. Roldán, M., et al., *Effect of helium implantation on mechanical properties of EUROFER97 evaluated by nanoindentation.* Journal of Nuclear Materials, 2014. **448**(1–3): p. 301-309.
10. Roldán, M., et al., *Comparative study of helium effects on EU-ODS EUROFER and EUROFER97 by nanoindentation and TEM.* Journal of Nuclear Materials, 2015. **460**(0): p. 226-234.

11. Lindau, R., et al., *Present development status of EUROFER and ODS-EUROFER for application in blanket concepts.* Fusion Engineering and Design, 2005. **75-79**: p. 8.

12. Marmy, P. and T. Kruml, *Low cycle fatigue of Eurofer 97.* Journal of Nuclear Materials, 2008. **377**(1): p. 52-58.

13. Tavassoli, F., *Eurofer Steel, Development to Full Code Qualification.* Procedia Engineering, 2013. **55**: p. 300-308.

14. Aktaa, J. and R. Schmitt, *High temperature deformation and damage behavior of RAFM steels under low cycle fatigue loading: Experiments and modeling.* Fusion Engineering and Design, 2006. **81**(19): p. 2221-2231.

15. Petersen, C., et al., *Tensile and low cycle fatigue properties of different ferritic/martensitic steels after the fast reactor irradiation 'ARBOR 1'.* Journal of Nuclear Materials, 2009. **386-388**: p. 299-302.

16. Walter, M., J. Aktaa, and M. Lerch, *Failure behaviour of EUROFER 97 in the low-cycle fatigue region under multi-step loading.* International Journal of Fatigue, 2008. **30**(3): p. 568-573.

17. Weick, M. and J. Aktaa, *Multiaxial fatigue behavior of EUROFER 97.* Journal of Nuclear Materials, 2007. **367-370**: p. 633-636.

18. Fernández, P., et al., *RAFM steel eurofer'97 as possible structural material for fusion device. Metallurgical characterization on as received condition and after simulated service conditions.* Inorme técnico CIEMAT, 2004.

19. Giordana, M.F., I. Alvarez-Armas, and A. Armas, *On the Cyclic Softening Mechanisms of Reduced Activity Ferritic/Martensitic Steels.* Steel Research International, 2012. **83**(6): p. 594-599.

20. Batista, M.N., et al., *Cyclic deformation and microstructural behaviour of reduced activation ferritic–martensitic steels.* Materials Science and Technology, 2014. **30**(14): p. 1826-1831.

21. Verma, P., et al., *Low cycle fatigue behavior of modified 9Cr–1Mo steel at room temperature.* Materials Science and Engineering: A, 2016. **652**: p. 30-41.

22. Klueh, R.L., K. Ehrlich, and F. Abe, *Ferritic martensitic steels promises and problems.* Journal of Nuclear Materials, 1992: p. 8.

23. Tavassoli, A.A.F., et al., *Current status and recent research achievements in ferritic/martensitic steels.* Journal of Nuclear Materials, 2014. **455**(1–3): p. 269-276.

24. Coffin, L.F.J., *A Study of the Effects of Cyclic Thermal Stresses on a Ductile Metal.* Transactions of the ASME, 1954. **76**: p. 11.

25. *Low Cycle Fatigue and Elasto-Plastic Behaviour of Materials.* 1987: Springer Science+Business Media B.V.

26. Smith, R.W., S.S. Manson, and M.H. Hirschberg, *Fatigue behavior of materials under strain cycling in low and intermediate life range.* Proceedings of the Tenth Sagamore Army Research Conference, 1964(NASA TN D-1574).

27. Wen, L.-c. and J.R.G. Ross, *Comparison of LCC Solder Joint Life Predictions With Experimental Data.* Journal of Electronic Packaging, 1995. **117**(2): p. 109-115.

28. Golanski, G., S. Mrozinski, and K. Werner, *Influence of temperature on low cycle properties of martensitic cast steel*, in *Archive of Mechanical Engineering.* 2012. p. 329.

29. Mishnev, R., N. Dudova, and R. Kaibyshev, *Low Cycle Fatigue Behavior of a 10% Cr Martensitic Steel at 600°C.* ISIJ International, 2015. **55**(11): p. 2469-2476.

30. Stubbins, J.F. and D.S. Gelles, *Fatigue performance and cyclic softening of F82H, a ferritic-martensitic steel.* Journal of Nuclear Materials, 1996. **233**: p. 331-335.

31. Zhang, Z., et al., *Low-Cycle Fatigue Properties of P92 Ferritic-Martensitic Steel at Elevated Temperature.* Journal of Materials Engineering and Performance, 2016. **25**(4): p. 1650-1662.

32. Armas, A.F., et al., *Mechanical and microstructural behaviour of isothermally and thermally fatigued ferritic/martensitic steels.* Journal of Nuclear Materials, 2002. **307**: p. 509-513.

33. ASM, *Fractography.* 6. print ed. ASM handbook. 2009, Materials Park, Ohio: ASM International. 517.

34. Fernández, P., et al., *Metallurgical characterization of the reduced activation ferritic/martensitic steel Eurofer'97 on as-received condition.* Fusion Engineering and design, 2001. **58-59**: p. 6.

35. Simm, T., et al., *The Influence of Lath, Block and Prior Austenite Grain (PAG) Size on the Tensile, Creep and Fatigue Properties of Novel Maraging Steel.* Materials, 2017. **10**(7): p. 730.

36. Białobrzeska, B., Ł. Konat, and R. Jasiński, *The Influence of Austenite Grain Size on the Mechanical Properties of Low-Alloy Steel with Boron.* Metals, 2017. **7**(1).

37. Fernández, P., et al., *TEM characterization on new 9% Cr advanced steels thermomechanical treated after tempering.* Journal of Nuclear Materials, 2018. **500**: p. 1-10.

38. Sauzay, M., et al., *Cyclically induced softening due to low-angle boundary annihilation in a martensitic steel.* Materials Science and Engineering: A, 2005. **400**: p. 241-244.

39. Kim, S. and J.R. Weertman, *Investigation of microstructural changes in a ferritic steel caused by high temperature fatigue.* Metallurgical Transactions A, 1988. **19**(4): p. 999-1007.

40. Armas, A.F., et al., *Cyclic instability of martensite laths in reduced activation ferritic/martensitic steels.* Journal of Nuclear Materials, 2004. **329**: p. 252-256.

41. Giordana, M.F., I. Alvarez-Armas, and A. Armas, *Microstructural characterization of EUROFER 97 during low-cycle fatigue.* Journal of Nuclear Materials, 2012. **424**(1): p. 247-251.

42. Materna-Morris, E., A. Möslang, and H.C. Schneider, *Tensile and low cycle fatigue properties of EUROFER97-steel after 16.3dpa neutron irradiation at 523, 623 and 723K.* Journal of Nuclear Materials, 2013. **442**(1, Supplement 1): p. S62-S66.

43. Paul, S.K., N. Stanford, and T. Hilditch, *Effect of martensite morphology on low cycle fatigue behaviour of dual phase steels: Experimental and microstructural investigation.* Materials Science and Engineering: A, 2015. **644**: p. 53-60.

44. Furuhara, T., et al., *Phase Transformation from Fine-grained Austenite.* ISIJ International, 2008. **48**(8): p. 1038-1045.

45. Mine, Y., et al., *Micro-tension behaviour of lath martensite structures of carbon steel.* Materials Science and Engineering: A, 2013. **560**: p. 535-544.

46. Jones, W.B., C.R. Hills, and D.H. Polonis, *Microstructural evolution of modified 9Cr-1Mo steel.* Metallurgical Transactions A, 1991. **22**(5): p. 1049-1058.

47. Wang, W., et al., *Effect of Thermal Aging on Microstructure and Mechanical Properties of China Low-Activation Martensitic Steel at 550 °C.* Nuclear Engineering and Technology, 2016. **48**(2): p. 518-524.

48.   Fernández, P., *Estudio de las propiedades metalúrgicas de los aceros martensíticos de activación reducida para su aplicación en los reactores de fusión.* Tesis doctoral, 2007.

49.   Chauhan, A., et al., *High-temperature low-cycle fatigue behavior of a 9Cr-ODS steel: Part 1 - pure fatigue, microstructure evolution and damage characteristics.* Materials Science and Engineering: A, 2017. **707**: p. 207-220.

50.   Shankar, V., et al., *Low cycle fatigue and thermo-mechanical fatigue behavior of modified 9Cr–1Mo ferritic steel at elevated temperatures.* Journal of Nuclear Materials, 2012. **420**(1): p. 23-30.

51.   Golański, G. and S. Mroziński, *Low cycle fatigue and cyclic softening behaviour of martensitic cast steel.* Engineering Failure Analysis, 2013. **35**: p. 692-702.

52.   Cottrell, A.H., *Dislocations and Platic Flow in Crystals*, ed. T.i.s.o.m.o. physics. 1954: Oxford at the Carendon Press. 223.

53.   Klueh, R.L. and A.T. Nelson, *Ferritic/martensitic steels for next-generation reactors.* Journal of Nuclear Materials, 2007. **371**(1-3): p. 37-52.

54.   Batista, M.N., et al., *The role of microstructure in fatigue crack initiation of 9–12%Cr reduced activation ferritic–martensitic steel.* International Journal of Fatigue, 2015. **72**: p. 75-79.

55.   Zeman, A., et al., *Microstructural analysis of candidate steels pre-selected for new advanced reactor systems.* Journal of Nuclear Materials, 2007. **362**(2): p. 259-267.

56.   Vitek, J.M. and R.L. Klueh, *Precipitation reactions during the heat treatment of ferritic steels.* Metallurgical Transactions A, 1983. **14**(6): p. 1047-1055.